

Leaky-Wave Radiation from a Slot The Time-Domain View

Lager, Ioan E.; Neto, Andrea; Štumpf, Martin

DO

10.23919/EuCAP63536.2025.10999195

Publication date 2025

Document VersionFinal published version

Published in

Proceedings of the 2025 19th European Conference on Antennas and Propagation (EuCAP)

Citation (APA)

Lager, I. E., Neto, A., & Štumpf, M. (2025). Leaky-Wave Radiation from a Slot: The Time-Domain View. In *Proceedings of the 2025 19th European Conference on Antennas and Propagation (EuCAP)* IEEE. https://doi.org/10.23919/EuCAP63536.2025.10999195

Important note

To cite this publication, please use the final published version (if applicable). Please check the document version above.

Copyright

Other than for strictly personal use, it is not permitted to download, forward or distribute the text or part of it, without the consent of the author(s) and/or copyright holder(s), unless the work is under an open content license such as Creative Commons.

Takedown policy

Please contact us and provide details if you believe this document breaches copyrights. We will remove access to the work immediately and investigate your claim.

Green Open Access added to <u>TU Delft Institutional Repository</u> as part of the Taverne amendment.

More information about this copyright law amendment can be found at https://www.openaccess.nl.

Otherwise as indicated in the copyright section: the publisher is the copyright holder of this work and the author uses the Dutch legislation to make this work public.

Leaky-Wave Radiation from a Slot: The Time-Domain View

Ioan E. Lager*, Andrea Neto*, Martin Štumpf[†],

*Delft University of Technology, 2628 CD Delft, the Netherlands, e-mail i.e.lager@tudelft.nl, a.neto@tudelft.nl,

†Brno University of Technology, 61600 Brno, the Czech Republic,
and with the EISLAB, Department of Computer Science, Electrical and Space Engineering,
Luleå University of Technology, 971 87 Luleå, Sweden, e-mail martin.stumpf@centrum.cz,

Abstract—A time-domain model of the leaky-wave radiation from a slot is assembled via an in-depth numerical investigation. The reported numerical experiments, all making use of a strictly causal excitation, provide a practical guideline for designing leaky-lens antennas (LLAs) and, above all, cogently elucidate the causal mechanism building up the propitious electromagnetic field distribution underpinning the LLA operation.

I. Introduction

Leaky-lens antennas (LLAs) count among the most effective (sub-)millimetre wave radiators [1]-[3], offering singular capabilities in applications ranging from ultra-high-rate digital communications to deep-space astronomical instrumentation. The operating principles of this device were described in [4] and rely on the foundations established in [5], [6]. In line with, practically, the entire literature on leaky-wave (LW) propagation (see the overview in [7]), the modelling of LLAs was done in frequency-domain (FD). Remarkably, until recently, the time-domain (TD) perspective on the LLA operation was missing. While the FD approach yielded a thorough understanding of the radiator's steady-state, time-harmonic (TH) operation and, mainly, extremely effective design tools, concerns were expressed in [8] about the adequacy of the FD models in ultra-high-rate systems, especially in combination with agile beam scanning, due to the increasingly short periods when a steady-state, TH excitation can be assumed. Another aspect that eluded examination referred to the lower limit of the gap height (see Section II-A) that still guarantees the type of electromagnetic (EM) radiation underpinning LLAs and, possibly, an optimum value of this geometric parameter.

To address this situation, [9] offered, for the first time, an analytical model of the *pulsed* EM radiation from a slot located in between a dielectric halfspace and a free-space one (henceforth referred to as **Gapless C.**). Subsequently, [10] discussed the radiation mechanism in **Gapless C.**, identifying the region between the first arrival of head-waves (HW) and the cone where body-wave (BW) propagation is possible as the support of LW radiation. Building on these results, [8] gave, via a careful numerical analysis, the first ever evidence of the qualitative difference between the HW–LW–BW (H-L-B) field distribution that characterises **Gapless C.**, and the "laminar" + conical beam (L+Cb) field distribution appearing in configurations in which the dielectric halfspace is elevated above the slot's plane (**Gap C.**), as encountered in LLAs.

The present work aims at *completing*, via numerical instruments, the TD description of the weakly-dispersive LW radiation from a slot. Firstly, the impact of the gap between the two halfspaces in **Gap C.** on the entailed EM field distribution will be investigated, the inspection of the transition from **H-L-B-** to **L+Cb-**type radiations yielding a minimum gap height needed for ensuring the predominance of the latter. Subsequently, the response of **Gap C.** to trains of pulses will be examined for seeking correlations between the EM field profile and the pulse repetition rate. Lastly, the response to short trains of pulses will be explored for identifying particularities in the EM field at the forefront and the tail of such a package, with the goal of understanding the effect of digital modulation in a carrier-based transmission. The account will be wrapped-up by formulating conclusions.

II. PREREQUISITES

A. Examined configuration

The configuration examined in this paper is the same as the one in [8] – the configuration shown in Fig. 1 coresponds to **Gap C.**, with **Gapless C.** being obtained by taking h=0. The relative permittivity in the dielectric halfspace is $\varepsilon_{\rm r}=16$. The slot width was w=1 mm. The domain of computation extends over -25 mm $\leqslant x \leqslant 25$ mm and -25 mm $\leqslant y \leqslant 25$ mm. The free-space lower half corresponds to -5 mm $\leqslant z < 0$ mm and the dielectric block to $h \leqslant z \leqslant h + 5$ mm. The gap height h took values between h=0 and h=0.7w. The field points A,\ldots,D in Fig. 1 were used in [11] for examining TD

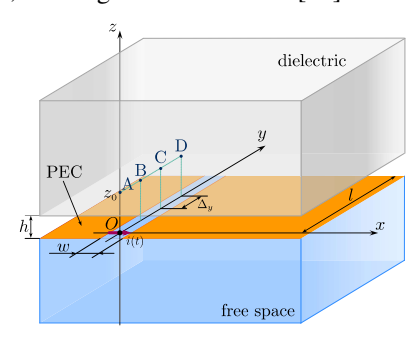


Fig. 1. Investigated configuration, comprising two homogeneous and isotropic half-spaces and a PEC sheet of negligible thickness in which a narrow slot is cut. The dielectric half-space is elevated from the PEC sheet by $h=\xi\,w$, with $0\leqslant\xi<2$. The slot is fed by a current-source-type port injecting a causal current pulse i(t). (The figure reproduces [8, Fig. 1].)

signatures and are preserved in this work as a reference for some of the discussed field snapshots.

All numerical experiments make use of the strictly causal, unipolar, windowed-power (WP) pulse [12]. The pulse's parameters are: pulse rising power $\nu=6$ and pulse width $t_{\rm w}=5\,{\rm ps}$ (entailing $s_{\rm w}=c_0t_{\rm w}=1.5\,{\rm mm}$, with c_0 denoting the free-space wavespeed), its signature being given in Fig. 2.a. Its spectral content peaks at DC, has the $-3\,{\rm dB}$ -point at $f=200\,{\rm GHz}$, the $-6\,{\rm dB}$ -point at $f=280\,{\rm GHz}$, and drops rapidly afterwards towards the first null at $f=600\,{\rm GHz}$ (all secondary lobes are under $-50\,{\rm dB}$).

B. Analysis methodology

As in [8], this analysis relies on simulations effectuated in CST Microwave Suite, this strategy offering an unparalleled possibility to perform experiments in a fully controlled environment, and at a level of detail that is out of reach for physical measurements. The numerical experiments employed a much finer mesh than that used in [8], the mesh-cells count being between 14,000,000 for Gapless C., and 14,400,000 for the largest gap height h. By effectively making use of the excitation's causality, all simulations were time-gated at 120 ps such that to completely preclude any boundary reflection in the region of interest (see [12] for details on the method). Despite the large mesh sizes, a full run took about 3 minutes on an Intel Xeon CPU 3.50 GHz / 128 GB workstation, with most computing time being taken by the post-processing phase. Additionally, self-developed Matlab code was used for the graphic post-processing of the CST computational data.

All subsequent plots represent $E_x(y,z)$ in the x=0 plane where, due to symmetry, is the only nonzero field component. As in [8], for compensating the effect of the high ε_r , we plot the $\varepsilon_r E_x$ quantity, normalised by $|\varepsilon_r E_x|_{\text{max}}$ (the maximum of

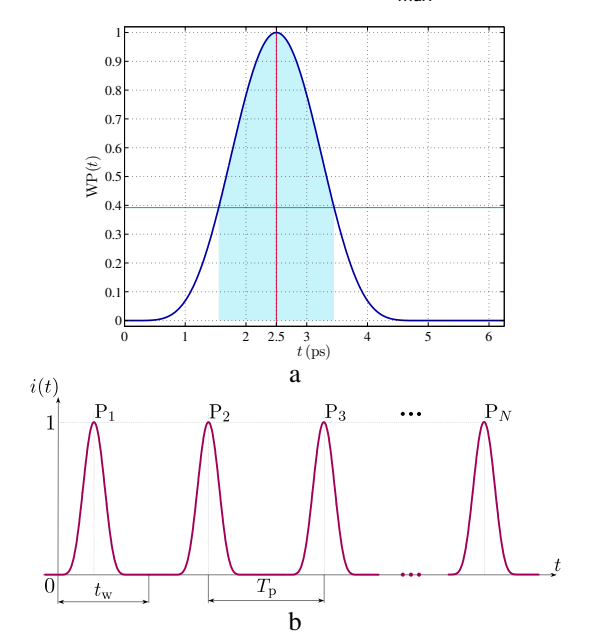


Fig. 2. Employed excitation. (a) The employed WP pulse shape; the shaded area between $t=1.55\,\mathrm{ps}$ and $3.45\,\mathrm{ps}$ accounts for 95% of the total pulse energy; (b) train of N identical WP pulses with pulse repetition period T_p .

 $|\varepsilon_{\rm r} E_x|$ over the shown snapshots). As demonstrated in [11], the response to the selected pulse shape approximates extremely well the configurational impulse response and, apart from the $\varepsilon_{\rm r}$ scaling, the given plots can also be construed as impulse response charts. The response to trains of pulses of the type in Fig. 2.b was synthesised by summing-up in Matlab successive CST-frames generated at regular intervals. By bearing in mind that the adopted field distributions are but approximations of the impulse response, the minimum pulse repetition period was taken as 3 ps, a choice justified by 95% of the pulse's total energy being concentrated within a 2 ps-long interval around the instant when the pulse peaks (see Fig. 2.a).

III. GAP-HEIGHT STUDY

The first study focused on the effect of the gap height h on the entailed pulsed-field response. To this end, h was varied from 0 to h=0.7w. The main results are shown in Fig. 3, with Fig. 3.a corresponding to **Gapless C.**, and Fig. 3.e to h=0.5w, *i.e.* the feature situation examined in [8]. The plots clearly evidence the gradual transition from the **H-L-B** field distribution in Fig. 3.a to the **L+Cb** one that was discussed in [8]. Some vestiges of **H-L-B** are still discernable for h=0.2w, but then rapidly fade away, with the **L+Cb** field distribution manifestly dominating already for h=0.4w. Accordingly, this gap height is a good practical lower limit for ensuring the type of EM propagation required by LLAs.

As in [8], the plots contain the following reference lines: the HW wavefront, the critical angle $\theta_{\rm c}$ for $\varepsilon_{\rm r}=16$, and the LW-related angle $\theta_{\rm c;L}$ given in [8, Eq. (7)]. As a novel element, the darker-green contour in these plots indicates the limit of the *significant*, CST-calculated values $(0.02|\varepsilon_{\rm r}E_x|_{\rm max}$ for **Gapless C.**, and $5\cdot 10^{-4}|\varepsilon_{\rm r}E_x|_{\rm max}$ for **Gap C.**), while the light-green contour delimits the region with *effectively-zero* values. The former contour illustrates the excellent correlation between the numerical results and the theoretical HW wavefront, while the latter contour presents further evidence for the remark made in [8, Section V] about small, but nonzero numerical data "travelling" at supraluminal velocities, an aspect that deserves a dedicated, in-depth investigation.

IV. PULSE REPETITION STUDY

The second study used the strategy in [8, Section IV-D], and amounted to superposing pulse responses at equally spaced instants, this equating to studying the configurational response to an excitation as in Fig. 2.b. Two tests were done:

- Examining the transition to a steady-state, (pulsed), periodic operation $(N \to \infty)$; to this end, all available CST generated frames, starting with the first nonzero response, were superimposed.
- Examining the on-off switching of a periodic, pulsed excitation, this replicating an elementary digital coding in a carrier-based transfer; to this end, the responses to N=4 and N=5 pulses were superimposed, and the TD evolution of the EM wave packet was monitored.

An example for the first type of analysis is given in Fig. 4 as a reference. It replicates the experiment reported in [8, Fig. 15.a]

and convincingly illustrates the significant improvement in the level of detail in the present work. As in all subsequent plots, the following reference lines are provided: the critical angle $\theta_{\rm c}$

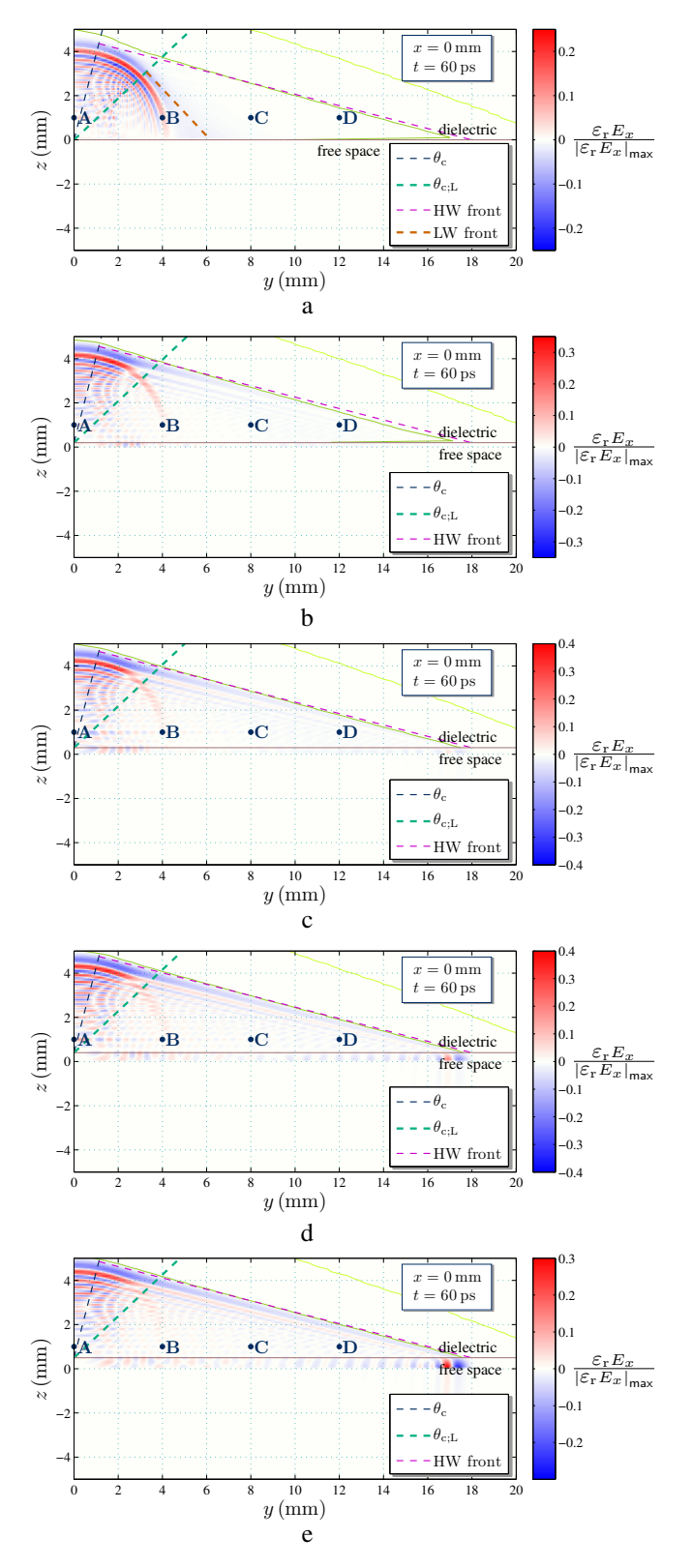


Fig. 3. Gap-height h analysis. (a) h=0 (Gapless C.); (b) h=0.2w; (c) h=0.3w; (d) h=0.4w; (e) h=0.5w.

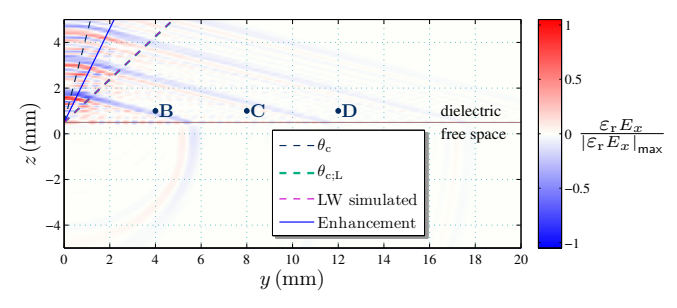


Fig. 4. Switched-on, steady-state, pulse repetition analysis for h=0.5w. The pulse repetition period is $T_{\rm p}=20\,{\rm ps}.$

for $\varepsilon_{\rm r}=16$, the LW-related angle $\theta_{\rm c;L}$, the simulated limit of the LW region (the limit of the "laminar" field distribution), and the field "Enhancement" (interpolating the locations of local field enhancement, this line being taken as representative for the shadow-boundary limit examined in [4]). Note that the $\theta_{\rm c;L}$ and LW simulated limit lines often (nearly) overlap.

A. Switched-on, steady-state, pulsed excitation

The first new experiment, reported in Fig. 5, employed a very short pulse repetition for h=0.5w. The obtained signatures have a high degree of uniformity, with the beam above the radiating port being either fuzzy ($T_{\rm p}=3\,{\rm ps}$) or featureless ($T_{\rm p}=5\,{\rm ps}$), none of them allowing determining an "Enhancement" line. It was then concluded that this pulse frequency is too high for being relevant for practical applications. Next, h=0.5w was maintained, but $T_{\rm p}$ was increased up to the one in Fig. 6. The beam started showing some clear profile that allowed determining the "Enhancement". However, the field distribution displays quite some variability, with only

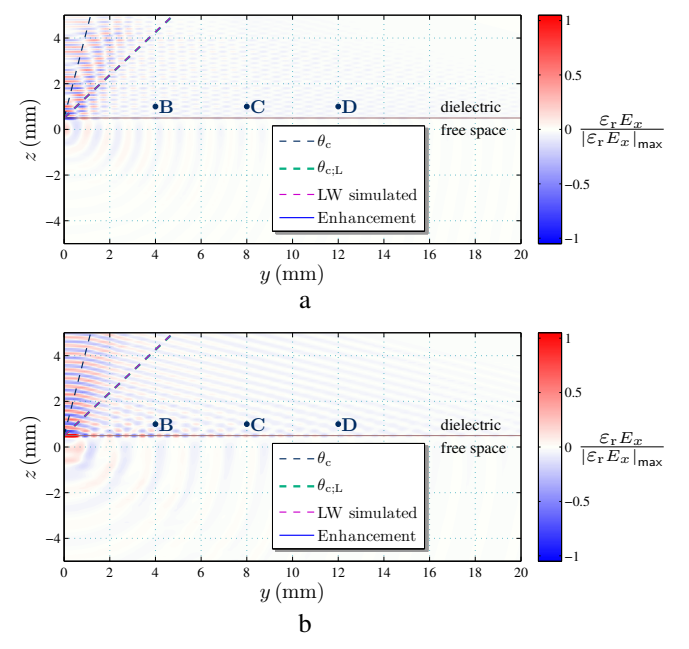


Fig. 5. Switched-on, steady-state, pulse repetition analysis for h=0.5w. The pulse repetition period is: (a) $T_{\rm p}=3\,{\rm ps}$; (b) $T_{\rm p}=5\,{\rm ps}$.

 $T_{\rm p}=11\,{\rm ps}$ offering the propitious combination of regularity and field enhancement for collimating a *steady-state* beam.

We can now formulate the main thesis of this work, namely that this analysis proves beyond any doubt that this weakly-dispersive LW radiation is the result of constructive or destructive interference of causal waves launched at regular intervals from a feeding point. This crucial observation falls completely outside the scope of any FD analysis that, inherently, cannot account for the origin of the field values at given locations. In no way do we question the validity of steady-state results inferred via FD instruments, we only demonstrate, for the first time, the mechanism leading to the observed steady-state field features. At the same time, we cogently illustrate the transition to the steady-state, in which period the obtained beam can differ a lot from the expected, settled, steady-state profile – a matter of concern during the design phase.

The impact on the gap height was also studied, those plots being omitted for brevity. A minor gap-induced variability was noticed, this further substantiating the constructive/destructive interference thesis: the variation of the free-space path directly above the feeding point was very small, while the propagation in "LW region" is not influenced by the gap height, once the L+Cb field distribution is reached at (see Fig. 3).

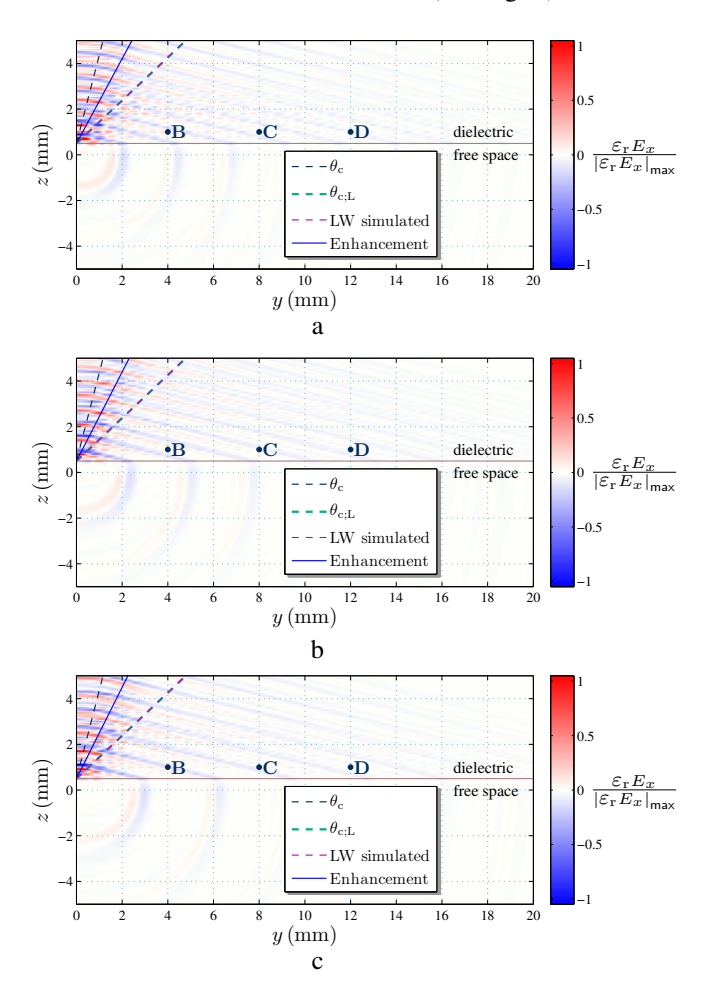


Fig. 6. Switched-on, steady-state, pulse repetition analysis for h=0.5w. The pulse repetition period is: (a) $T_{\rm p}=8\,{\rm ps}$; (b) $T_{\rm p}=9\,{\rm ps}$; (c) $T_{\rm p}=11\,{\rm ps}$.

TABLE I
ENHANCEMENT ANGLE DEPENDENCE ON THE GAP HEIGHT.

Gap height h	Enhancement angle	Standard deviation	Normalised standard deviation
0.3w	30.6°	0.899°	2.94%
0.4w	29.3°	0.937°	3.20%
0.5w	27.2°	1.184°	4.35%
0.6w	24.3°	1.118°	4.60%
0.7w	24.0°	1.099°	4.58%

Another aspect noticed in [11] was that the "Enhancement" line moves closer to the z-axis as h increases, an evolution in striking accordance with the shadow-boundary analysis in [4]. The data in Table I confirms that observation even for the reduced range of gap heights examined in this work. Note that the currently inferred angles slightly differ from those reported in [11], which is understandable in view of the substantially improved accuracy in the present simulations.

B. Time-windowed, pulsed excitation

Upon again taking h=0.5w in cojunction with $T_{\rm p}=11$ ps, the evolution of *time-windowed* trains of pulses was examined in Figs. 7 and 8 for the cases of 4 and 5 consecutive feeding pulses, respectively. The previously used reference lines were preserved for facilitating comparisons. These signatures are indicative for the large transformation that the EM wave packet undergoes, with some snapshots displaying field distributions in which *no beam is discernable anymore*! While this analysis is clearly qualitative, it definitely raises serious concerns on the feasibility of using *steady-state-*based results in the design of digitally-coded wireless channels — evidently, each kind of digital carrier modulation will have a different impact on the effectively obtained field distribution.

V. CONCLUSIONS

A TD model of the weakly-dispersive, LW radiation in LLAs was discussed. The minimum air gap between the slot and the dielectric half-space was inferred. By superposing successive, equally-spaced, EM field frames it was demonstrated that the EM radiation is the result of constructive/destructive interference of causal waves that, *as an ensemble* provide the features given by FD instruments. Finally, it was shown that short wave packages display widely variable field distributions, this raising concerns about the suitability of FD results in the case of digitally-modulated, carrier-based transmissions.

REFERENCES

- N. Llombart, G. Chattopadhyay, A. Skalare, and I. Mehdi, "Novel terahertz antenna based on a silicon lens fed by a leaky wave enhanced waveguide," *IEEE Trans. Antennas Propag.*, vol. 59, no. 6, pp. 2160– 2168, Jun. 2011.
- [2] A. Neto, N. Llombart, J. J. A. Baselmans, A. Baryshev, and S. J. C. Yates, "Demonstration of the leaky lens antenna at submillimeter wavelengths," *IEEE Trans. THz Sci. Technol.*, vol. 4, no. 1, pp. 26–32, Jan. 2014.
- [3] S. van Berkel, E. S. Malotaux, C. De Martino, M. Spirito, D. Cavallo, A. Neto, and N. Llombart, "Wideband double leaky slot lens antennas in CMOS technology at submillimeter wavelengths," *IEEE Trans. THz Sci. Technol.*, vol. 10, no. 5, pp. 540–553, Sep. 2020.

- [4] A. Neto, "UWB, non dispersive radiation from the planarly fed leaky lens antenna Part 1: Theory and design," *IEEE Trans. Antennas Propag.*, vol. 58, no. 7, pp. 2238–2247, Jul. 2010.
 [5] A. Neto and S. Maci, "Green's function for an infinite slot printed
- [5] A. Neto and S. Maci, "Green's function for an infinite slot printed between two homogeneous dielectrics – Part I: Magnetic currents," *IEEE Trans. Antennas Propag.*, vol. 51, no. 7, pp. 1572–1581, Jul. 2003.
- [6] S. Maci and A. Neto, "Green's function for an infinite slot printed between two homogeneous dielectrics – Part II: Uniform asymptotic solution," *IEEE Trans. Antennas Propag.*, vol. 52, no. 3, pp. 666–676, Mar. 2004.
- [7] D. R. Jackson, P. Burghignoli, G. Lovat, F. Capolino, J. Chen, D. R. Wilton, and A. A. Oliner, "The fundamental physics of directive beaming at microwave and optical frequencies and the role of leaky waves," *Proc. IEEE*, vol. 99, no. 10, pp. 1780–1805, Oct. 2011.
- [8] J. Gu, M. Štumpf, A. Neto, and I. E. Lager, "Pulsed operation of a weakly dispersive, leaky wave antenna: A causal numerical study," *IEEE*

- Trans. Antennas Propag., vol. 72, no. 1, pp. 720-732, Jan. 2024.
- [9] M. Štumpf, J. Gu, and I. E. Lager, "Time-domain electromagnetic leaky waves," *IEEE Trans. Antennas Propag.*, vol. 71, no. 4, pp. 3382–3392, Apr. 2023.
- [10] J. Gu, A. Neto, I.E. Lager, and M. Štumpf, "Wave-front behaviour of the pulsed EM field – Complexity and implications," in *Proc.* 17th EuCAP, 2023.
- [11] J. Gu, M. Štumpf, A. Neto, and I.E. Lager, "Pulsed operation of a weakly dispersive, leaky wave antenna: A causal numerical study," Supplementary material, *IEEE Trans. Antennas Propag.*, doi: 10.1109/TAP.2023.3338006/mm1.
- [12] I. E. Lager and S. L. van Berkel, "Finite temporal support pulses for EM excitation," *IEEE Antennas Wireless Propag. Lett.*, vol. 16, pp. 1659– 1662, Jun. 2017.

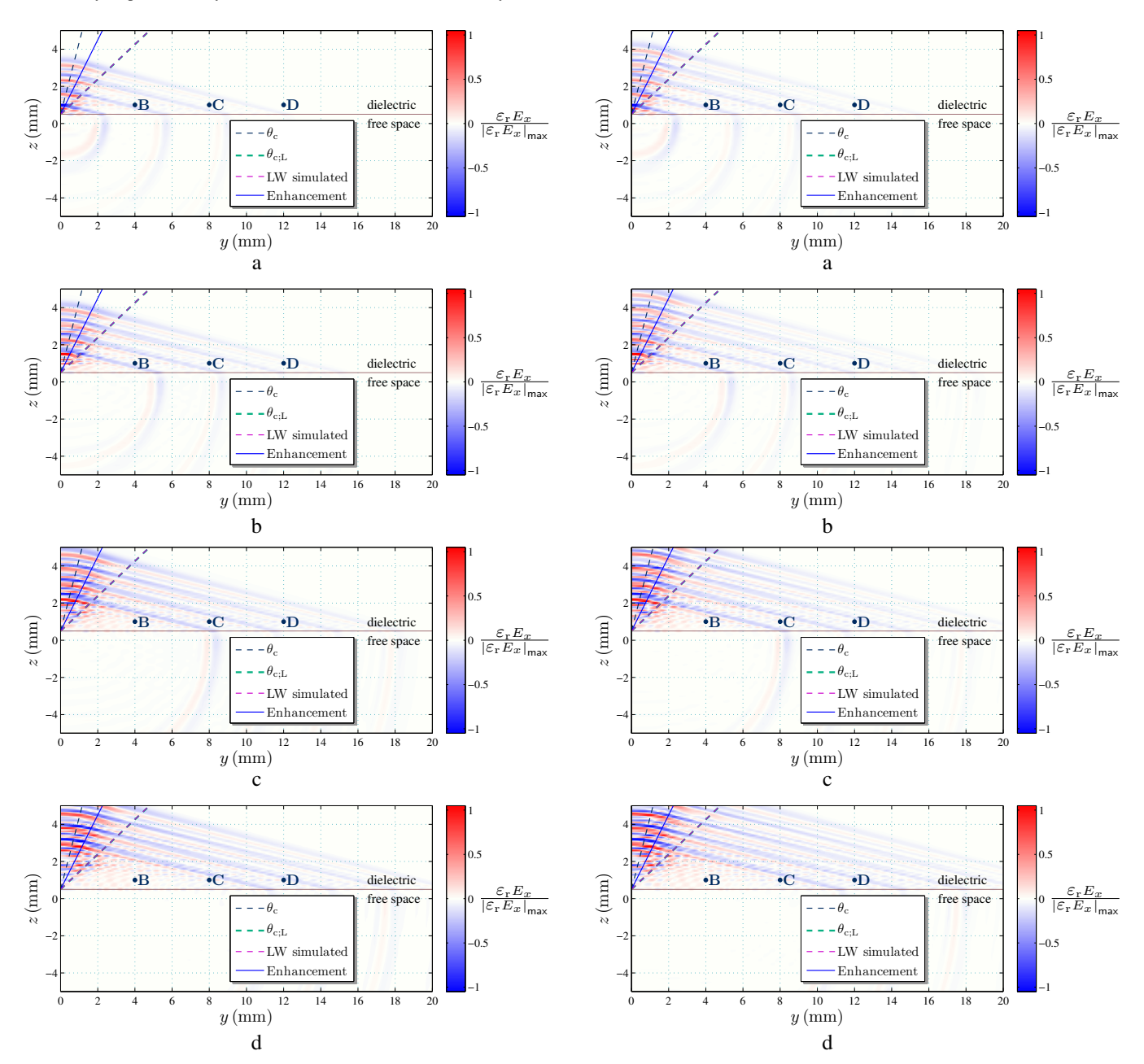


Fig. 7. Time-windowed, analysis for h=0.5w, and 4 consecutive pulses at $T_{\rm p}=11$ ps. Field snapshots at: (a) t=43 ps; (b) t=53 ps; (c) t=63 ps; (d) t=73 ps.

Fig. 8. Time-windowed, analysis for h=0.5w, and 5 consecutive pulses at $T_{\rm p}=11~{\rm ps}$. Field snapshots at: (a) $t=54~{\rm ps}$; (b) $t=64~{\rm ps}$; (c) $t=74~{\rm ps}$; (d) $t=84~{\rm ps}$.